CrystEngComm

RSC Publishing

PAPER

View Article Online
View Journal | View Issue

Cite this: *CrystEngComm*, 2013, **15**, 4739

Annealing-induced ultra-efficient NIR-to-VIS upconversion of nano-/micro-scale α and β $NaYF_4:Er^{3+},Yb^{3+}$ crystals†

Hassane Assaaoudi, Guo-Bin Shan, Nathan Dyck and George P. Demopoulos*

Received 28th February 2013,
Accepted 25th April 2013

DOI: 10.1039/c3ce40362a

www.rsc.org/crystengcomm

Nano-/micro-scale α and β $NaYF_4:Er^{3+},Yb^{3+}$ crystals with ultra-efficient upconversion (UC) of near infrared (NIR)-to-visible (VIS) light were prepared by annealing following citrate-assisted hydrothermal synthesis at 200 °C. Excess fluoride ([F]/[Y + Er + Yb] molar ratio = 9) helped promote the formation of the hexagonal β phase while simultaneous addition of citrate led to crystal shape and size control. The citrate caused the morphology of the β phase crystals to change from irregular elongated microtubes to hexagonal prisms, with particle size decreasing with increasing citrate concentration. However the presence of citrate led to significant deterioration of the upconversion luminescence of the β $NaYF_4:Er^{3+},Yb^{3+}$ crystals due to surface quenching by adsorbed citrate moieties. We have found that annealing at 700 °C restored the NIR-to-VIS upconversion luminescence (predominantly green) of the citrate-modified β $NaYF_4:Er^{3+},Yb^{3+}$ crystals and also led to a dramatic enhancement (over several orders of magnitude) not previously reported. According to Raman spectroscopic evidence, annealing led to improved upconversion efficiency *via* elimination of internal defects and surface hydroxyl/citrate groups. Further, we report on the preparation of unexpectedly strong upconverting (predominantly red) α cubic phase $NaYF_4:Er^{3+},Yb^{3+}$ nanocrystals.

1 Introduction

Nanoengineering of upconversion materials[1] currently attracts a great deal of attention due to their great potential in several advanced applications including optical devices,[2] data storage,[3] biomedical imaging and labeling[4] and photovoltaics.[5] Upconversion materials, which commonly are rare-earth (RE)-doped compounds, convert two or more low energy photons to a single higher energy photon.[6] Among these optical materials, $NaYF_4:Er^{3+},Yb^{3+}$, with Yb^{3+} as sensitizer and Er^{3+} as activator, is recognized as one of the most promising NIR-to-VIS upconverters.[2,7] Under the excitation of 980 nm light, this upconverter emits green (510–570 nm) and red (640–680 nm) light, the relative intensity of which is reported to be affected by crystal phase, size, shape, and doping. It has been widely accepted that the β-hexagonal crystal phase $NaYF_4:Er^{3+},Yb^{3+}$ (doped with 2 mol% Er^{3+} and 18 mol% Yb^{3+}) exhibits superior upconversion efficiency compared to its α-cubic counterpart (approximately 10 times stronger green emission and 4–5 times stronger total emission).[8] Crystal size is also important as nanocrystals are reported to exhibit lower upconversion luminescence than bulk crystals due to higher occurrence of surface quenching sites.[2,9]

A common method used to control the shape and size of $NaYF_4:Er^{3+},Yb^{3+}$ upconverting crystals is the use of crystal modifying agents, such as oleic acid,[2,10,11] EDTA or sodium citrate[12] in conjunction with solvothermal or hydrothermal synthesis. According to Zhang *et al.*[11] the upconversion emission intensity of Er^{3+},Yb^{3+}-doped-hexagonal nanocrystals (nanorods, nanotubes or nanodiscs prepared with oleic acid) was as much as 50% lower than the corresponding one of bulk crystals of the same composition. Sun *et al.*[12a] used a hydrothermal method to prepare citrate-modified micron-sized hexagonal shaped β $NaYF_4:Er^{3+},Yb^{3+}$ crystals whose upconversion was rather weak and dominated by the red band. New reports focusing on nanocrystal modification such as Gd substitution for Y in $NaYF_4:Er^{3+},Yb^{3+}$ or core–shell nanostructured particles have mitigated the loss of upconversion luminescence in nanocrystals but more work remains to be done.[1a,2]

The scope of the present work is to demonstrate that annealing of citrate-modified $NaYF_4:Er^{3+},Yb^3$ crystals can provide a powerful and easily implemented tool in achieving multi-fold enhancement of upconversion luminescence. $NaYF_4:Er^{3+},Yb^{3+}$ crystals were prepared with and without citrate by hydrothermal synthesis at 200 °C and subsequently annealed at 350 and 700 °C for 2 h. The upconversion luminescence of both α and β-$NaYF_4:Er^{3+},Yb^{3+}$ crystals can be greatly enhanced annealing at 700 °C and the green-to-red ratio can be tuned by proper selection of fluoride and citrate

Department of Materials Engineering, McGill University, Montreal, Canada. E-mail: george.demopoulos@mcgill.ca; Fax: +1-514-2984492; Tel: +1-514-3982046

† Electronic supplementary information (ESI) available. See DOI: 10.1039/c3ce40362a

concentrations. Detailed Raman spectroscopic analysis in addition to other characterization methods is used to explain the beneficial effects realized through annealing.

2 Experimental sections

2.1 Crystal preparation

The optimum co-dopant ratio for strongly efficient NIR to VIS upconversion has been found to be 2 mol% Er^{3+} and 18 mol% Yb^{3+} [8] and was therefore selected as the co-dopant ratio for our $NaYF_4$:Er^{3+},Yb^{3+} crystals. In a typical synthesis test, $Er(NO_3)_3{\cdot}5H_2O$ (0.04 mmol), $Yb(NO_3)_3{\cdot}5H_2O$ (0.36 mmol), and $Y(NO_3)_3{\cdot}6H_2O$ (1.6 mmol) were added into 40 mL deionized water (optionally adding 2.3, 13.7 or 54 mmol of sodium citrate dihydrate), followed by the addition of sodium fluoride (8 (corresponding to stoichiometric ratio: [F]/[Y + Er + Yb] = 4) or 18 mmol), and stirring for 15 min. The mixed solution was transferred into a stainless steel pressure vessel with Teflon-liner (125 mL, supplied by Parr Instruments) and heated to 200 °C for 2–24 h. The precipitate was separated by centrifugation, washed with deionized water three times, once with ethanol, and finally dried in air at 60 °C for 24 h. Various samples with different morphologies were prepared. For the present study, eight types are selected including three prepared without citrate (samples #1–#3) and five prepared with citrate (samples C1–C5) (see details in Table 1). To enable ultra-efficient upconversion response, the as-prepared crystals were annealed at 350 °C or 700 °C for 2 h, and then cooled to room temperature.

2.2 Characterization

The powders obtained were characterized by X-ray powder diffraction (XRD), field emission scanning electron microscopy (FE-SEM), transmission electron microscopy (TEM), as well as Fourier transform infrared (FTIR), Raman and luminescence spectroscopies. XRD analysis was performed on a Rigaku Rotaflex D-Max diffractometer equipped with a rotating anode, a copper target (λ(Cu Kα) = 1.5406 Å), a monochromator composed of a graphite crystal and a scintillator detector. The diffractometer used 40 kV and 20 mA. Scanning took place between 10° and 90° (2θ) with a 0.1° step and an acquisition time of 10 seconds per step. SEM images were obtained using a Hitachi S-4700 FE-SEM. TEM images were obtained using a Philips CM-200 microscope operating at 200 kV. Upconversion luminescence spectra were measured at room temperature on a Fluoromax-2 spectrophotometer by using a 980 nm laser (UH5 100G-980, 100 mW, World Star Tech) to replace the A-1010 arc lamp. The fluorescence was measured using powder samples; the laser spot size was kept the same when comparing samples, ensuring that the interaction volume and laser intensity was the same from sample to sample. The measurement spectra of all samples are recorded under the same conditions. The position of the laser relative to the samples was identical during all measurements. Each sample was immobilized and pressed between two glass slides to ensure a flat surface and fixed using a metallic sample holder. All annealed samples were ground using a mortar and pestle prior to measurement to minimize particle size differences and uneven surfaces. Upconversion luminescence was quantified by integrating the emission peaks from the obtained spectra. For simpler comparison purposes, integration values were presented as a ratio in comparison with a reference sample (sample 2, see Table 2).

Infrared spectra were obtained using a Perkin Elmer FTIR (Spectrum BX model) spectrometer with a Miracle single bounce diamond ATR cell from PIKE Technologies. Spectra over the mid-IR (4000–550 cm^{-1}) range were obtained by the co-addition of 16 scans with a resolution of 4 cm^{-1}. Spectral treatment such as baseline adjustment, ATR correction and data collection were performed using the Spectrum software (version 5.02) from Perkin Elmer.

The Raman spectra were collected with an InVia Raman microscope from Renishaw using a polarized He–Ne laser operating at 514 nm. The laser delivered 7.2 mW at the laser exit and the power density was 6.75 mW μm^{-2} at the sample, using a 20× distance objective. Only one scan was collected from 150 to 4000 cm^{-1}. The energy resolution was 4 cm^{-1} at the full width at half maximum of the internal Si reference peak. The scans were collected at 0.5% of the laser output at the microscope exit to avoid radiation damage. Each crystal sample, in addition, was inspected with the microscope objective after each scan. The system was calibrated to the 520 cm^{-1} silicon peak (for position and intensity) before the collection of any data. Spectral treatment was performed with the WiRE 2.0 software from Renishaw.

Table 1 Different type of $NaYF_4$:Er^{3+},Yb^{3+} crystals prepared hydrothermally by varying the NaF and citrate contents (T = 200 °C; {Y + Er + Yb} = 2 mmol)

				$NaYF_4$ crystals		
Samples	NaF (mmol)	Citrate (mmol)	Time [h]	Phase	Shape	Average size (dimensions, nm)
#1	8	0	2	α	Spheroidal agglomerates	~200–600 (D)
#2	18	0	2	β	Irregular microtubes	~500 (D) × 1500 (L)
#3	8	0	24	β	Microtubes	~1000 (D) × 3000–6000 (L)
C1	8	2.3	24	α	Nanoparticles	~15–30 (D)
C2	18	2.3	3	β	Hexagonal microprisms	~1200–2000 (D) × 800–1000 (L)
C3	18	2.3	24	β	Hexagonal microprisms	~1600–2900 (D) × 1000–1400 (L)
C4	18	13.7	2	β	Hexagonal nanoprisms	~300–500 (D) × 250–300 (L)
C5	18	54	2	β	Nanobarrels	150–200 (D)

Table 2 Upconversion properties of various $NaYF_4:Er^{3+},Yb^{3+}$ crystal samples following hydrothermal synthesis (as-prepared) and after annealing at 350 °C and 700 °C for 2 h

T	Samples	Total emission (a.u.)	Annealing-induced increase of total emission (times)	Green (a.u.)	Red (a.u.)	The green-to-red ratio
As-prepared	1	0.05	—	0.04	0.05	0.75
	2[a]	1.00	—	1.00	1.09	0.91
	3	0.48	—	0.29	0.69	0.42
	C1	0.10	—	0.09	0.09	0.97
	C2	0.21	—	0.28	0.17	1.50
	C3	0.59	—	0.77	0.43	1.81
	C4	0.11	—	0.12	0.09	1.39
	C5	0.02	—	0.02	0.01	2.21
350 °C	1	8.93	162.3	2.35	16.39	0.14
	2	25.45	25.5	21.41	32.04	0.67
	3	1.62	3.4	0.63	2.78	0.23
	C1	0.05	0.5	0.03	0.05	0.51
	C2	1.03	4.8	1.00	1.16	0.86
	C3	0.39	0.7	0.39	0.43	0.90
	C4	4.32	40	4.04	5.03	0.80
	C5	4.21	191.4	2.67	6.16	0.43
700 °C	1	57.50	1045.5	30.67	90.13	0.34
	2	43.57	43.6	25.16	66.41	0.38
	3	29.34	61.1	6.92	54.60	0.13
	C1	60.92	591.4	20.60	107.34	0.19
	C2	53.69	250.9	60.00	52.74	1.14
	C3	47.67	81.3	50.01	50.02	1.00
	C4	19.48	180.4	21.50	19.40	1.11
	C5	90.17	4098.5	101.63	87.49	1.16

[a] Reference sample.

3 Results and discussion

3.1 Hydrothermal synthesis and upconversion properties of $NaYF_4:Er^{3+},Yb^{3+}$ crystals

3.1.1 Citrate-assisted crystal phase, size and morphology control. By varying the NaF concentration, hydrothermal time, and the amount of citrate, the nucleation and growth of $NaYF_4:Er^{3+},Yb^{3+}$ was altered leading to production of different types of crystals as summarized in Table 1. XRD patterns of several crystal samples (#1, C1, C2, C3, C5) are shown in Fig. S1 (in ESI†). Both #1 and C1 are characteristic of a pure cubic phase (space group: $Fm\bar{3}m$), which matches with standard cubic $NaYF_4$ XRD pattern (JCPDS No. 04-008-3252). Their calculated lattice constant (*a*) is 5.4480(10) Å.[13] The XRD patterns of samples C2 through C5 are similar to each other (Fig. S1, ESI†) and can be indexed to pure hexagonal phase (space group: $P\bar{6}$ or $P6_3/m$), in good agreement with the JCPDS 04-010-4420. Their calculated lattice constants are: a = 5.6022(2) Å and c = 3.3295(2) Å (JCPDS: 04-011-3583).[14]

In the absence of sodium citrate, with a stoichiometric amount of NaF (*i.e.* 8 mmol NaF or [F]/[Y + Er + Yb] = 4), and with hydrothermal treatment of 200 °C for 2 h, cubic structure (α) $NaYF_4:Er^{3+},Yb^{3+}$ crystals were produced in the form of submicron sized spheroidal agglomerates. By increasing the reaction time to 24 h, the cubic phase (α) agglomerates (sample #1) were converted to hexagonal phase (β) elongated microtubes (sample #3), indicating crystal conversion was accompanied by crystal growth (see Fig. 1 and Table 1). From this, it is deduced that in the absence of citrate, spontaneous (homogeneous) nucleation of the kinetically favoured cubic (α) phase occurs and undergoes growth *via* primary particle aggregation leading to formation of spheroidal agglomerates.[15] Upon extension of hydrothermal reaction time the metastable cubic phase transform to the thermodynamically stable hexagonal phase. Repeating test #1 in the presence of citrate (2.3 mmol) produced no crystals after 2 h reaction time. This is attributed to the chelating ability of citrate to form bidentate and tridentate complexes with yttrium,[16] which delays the onset of nucleation. The presence of citrate also blocked particle growth, aggregation and transformation in the 24 h hydrothermal sample (sample C1 in Fig. 1), resulting in uniformly dispersed cubic phase nanoparticles of about 20 nm (see TEM picture in Fig. 1). The XRD peaks of sample C1 (α-$NaYF_4:Er^{3+},Yb^{3+}$) are broader than those of sample #1 (α-$NaYF_4:Er^{3+},Yb^{3+}$) (Fig. S1, ESI†), indicating the primary crystallite size of sample C1 is smaller, further illustrating the growth inhibition due to citrate. This can be attributed to citrate's role as crystal modifying agent as has been similarly shown for other yttrium compound crystals such as $YVO_4:Eu$[16] or β-$NaLuF_4$.[12c]

The crystallization kinetics change when NaF is added in excess (18 mmol corresponding to F/RE molar ratio = 9). Under these conditions, no α-phase crystals were produced. Sample #2 showed hexagonal (β) crystal structure even with reaction times as short as 2 h (see Table 1). Preferential formation of hexagonal phase due to excess fluoride is in line with previous hydrothermal synthesis studies involving mixed ethanol–water solvents.[9,17]

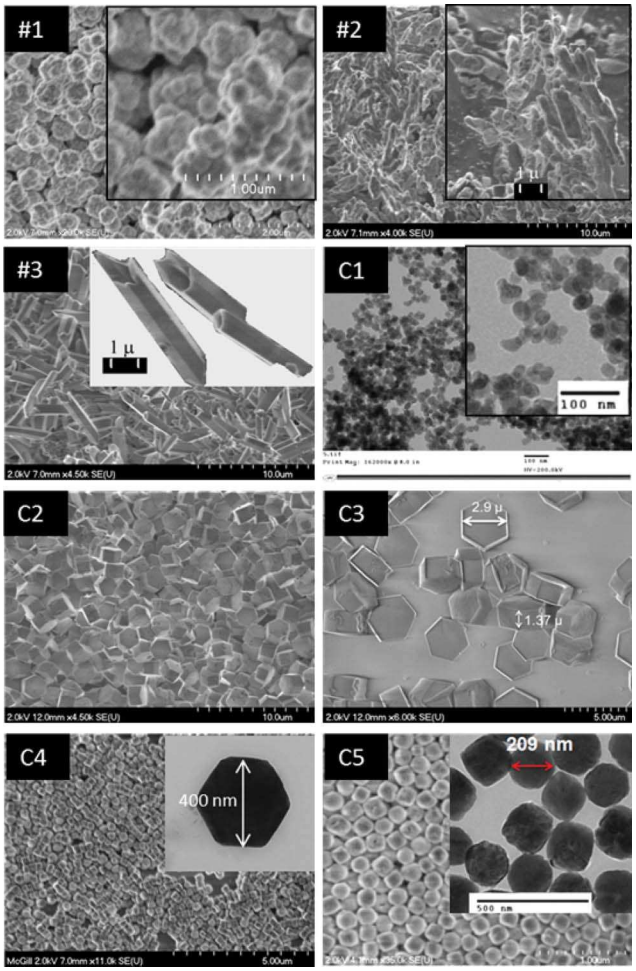

Fig. 1 SEM or TEM images of various $NaYF_4$:Er^{3+},Yb^{3+} crystal modifications (prior to annealing).

It is postulated that due to higher supersaturation associated with excess fluoride concentration, a faster homogeneous nucleation rate yielded smaller α-phase nuclei[18] that quickly (within the 2 h synthesis time) transformed to β-phase. Similarly no α-phase crystals were produced when NaF was in excess (18 mmol) in the presence of citrate (2.3 mmol, sample C2 in Table 1). However, shortening the reaction time to 1 h did produce α-phase nanocrystals (~15–20 nm; data not shown) confirming the postulated mechanism of particle growth.

The α-to-β phase transition has the characteristics of a dissolution–recrystallization mechanism.[19] As discussed by Zhang *et al.*[11] in connection to the analogous oleic acid-based hydrothermal system, the homogeneously nucleated, metastable α nanoscale crystallites, are restructured *via* dissolution to β-phase seed crystallites that subsequently grow in response to the relative reactivity of their anisotropic planes. The small hexagonal cylindrical shape seed crystals initially formed in the absence of citrate (samples #2 and #3 in Fig. 1), underwent preferential (1D) growth along the {0001} directions that led to the tube-like elongated structures.[19] In the presence of citrate, however the β crystal growth mechanism is altered, favouring (2D) hexagonal prisms (samples C2–C4). This occurs *via* selective adsorption of citrate on the {0001} facets.[19,20] The adsorption of citrate was confirmed by FTIR spectroscopy as evidenced by the characteristic peaks at ~1590 cm^{-1} (C=O stretch), 1400 cm^{-1} and ~900 cm^{-1} (O–H bend), and ~3300–3400 cm^{-1} (O–H stretch) in Fig. S2 (ESI†). Increasing the amount of sodium citrate, further inhibited β-phase crystal growth resulting in isometric morphology and size reduction, giving equi-axed submicron particles (0.2 µm) (see sample C5 in Fig. 1). The crystal modifying effect of citrate (Cit) on β-$NaREF_4$:Er^{3+},Yb^{3+} (where RE = Y or Lu) crystal growth was also reported by Sun *et al.*[12a] and Li *et al.*[12c] However, the latter researchers did not explore a wide range of citrate concentrations as done here and their produced crystals of microplate shape were rather large between 2 and 5 µm diameter. Their microplates were produced with ~1/1 molar ratio Cit/RE and large excess of F: F/RE = ~12. By using a ~25-fold higher citrate content (molar ratio Cit/RE = 54/2 and F/RE = 9) than in previous studies[12a,c] 3-D isotropic nanoscale β-$NaREF_4$:Er^{3+},Yb^{3+} crystals can be produced that are easier to suspend in solution for various applications.

3.1.2 Raman and upconversion spectra.

3.1.2.1 Raman spectra. We used Raman spectroscopy to compare α- and β-doped $NaYF_4$:Er^{3+},Yb^{3+} as well as doped and undoped crystals in an effort to reveal the optical-structural relations governing each phase. Representative spectra are shown in Fig. 2, while all spectra and Raman spectra data (cm^{-1}) of doped α- and β-$NaYF_4$:Er^{3+},Yb^{3+} crystals are reported respectively in Fig. S3 and Table S1 in the ESI.† This demonstrates, for the first time to the best of our knowledge, that Raman spectroscopy can be used as a tool to distinguish between α- and β-phase in doped $NaYF_4$:Er^{3+},Yb^{3+} crystals. It is interesting to note that under the laser excitation conditions applied, no Raman peaks were observed in the undoped hydrothermally synthesized $NaYF_4$ samples (Fig. 2). The spectra of doped α-$NaYF_4$:Er^{3+},Yb^{3+} (Fig. S3 in ESI†) show broadened peaks with medium intensities respectively within (1384–1416) cm^{-1} and (1041–932) cm^{-1}, as well as two other weak peaks near (703–687 cm^{-1}) and (279–260 cm^{-1}) cm^{-1}.

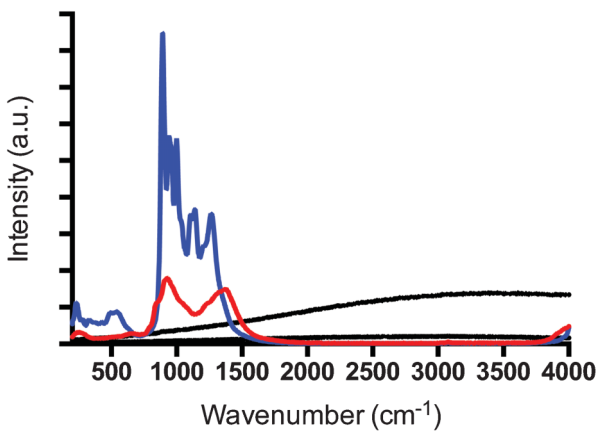

Fig. 2 Raman spectra of as-prepared α-$NaYF_4$:Er^{3+},Yb^{3+} (sample #1 red), β-$NaYF_4$:Er^{3+},Yb^{3+} (sample #2, blue), and undoped samples (black).

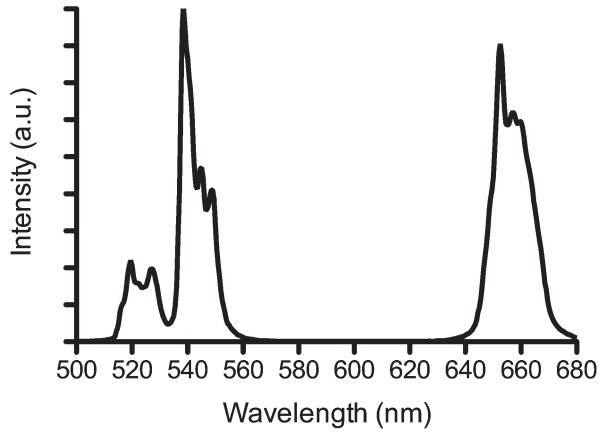

Fig. 3 Upconversion emission spectrum of citrate-free β-$NaYF_4$:Er^{3+},Yb^{3+} crystals (sample #2) following hydrothermal synthesis (as-prepared). This spectrum was used as basis for comparison.

The spectra of the β-$NaYF_4$:Er^{3+},Yb^{3+} (Fig. S3 in ESI†) show 5 very strong peaks characteristic of this form (along two or three more shoulder peaks) observed in the (1285–888 cm^{-1}) frequency range. Other peaks with weak intensities in the range of 230 to 580 cm^{-1} (listed in Table S1 in the ESI†) show fair agreement with reported values in literature.[21] The strong peaks in the range of (1285–888 cm^{-1}) observed in doped β-$NaYF_4$:Er^{3+},Yb^{3+} crystals are reported for the first time. These unique Raman peaks can be advantageously used to distinguish between cubic and hexagonal phases. In addition, the position and intensity of these peaks are related to UC luminescence as is shown later in connection to the effect of annealing (section 3.2).

3.1.2.2 Upconversion spectra. Under excitation at 980 nm, all $NaYF_4$:Er^{3+},Yb^{3+} samples yielded green emission at 510–570 nm and red emission at 640–680 nm, with emission intensity varying greatly depending on the synthesis and annealing conditions. Fig. 3 shows a typical upconversion luminescence spectrum (sample #2; prepared without use of citrate). This spectrum was used as reference to compare upconversion fluorescence of all other samples. The upconversion properties of the unannealed and annealed samples are summarized in Table 2. The hexagonal (β-$NaYF_4$:Er^{3+},Yb^{3+}) crystals exhibit stronger upconversion response than their cubic (α) counterpart (see samples #1 and C1 in Table 2). Citrate was found to have a negative effect on the upconversion luminescence (total emission) of the hydrothermally synthesized hexagonal crystals (β-$NaYF_4$:Er^{3+},Yb^{3+}). By examining the total emission of samples #2, C2, C4, and C5 in Table 2, we observe a gradual decrease in upconversion luminescence with increasing citrate content: total emission decreases from 1.00 (sample #2, no citrate) to 0.21 (sample C2), 0.11 (sample C4), and finally 0.02 (sample C5) as citrate increases from 2.3, to 13.7, and 54 mol respectively. This implies that the presence of citrate caused a quenching effect on upconversion response. This decrease in upconversion intensity may also be linked to the decreasing size (and morphology change) of the β-$NaYF_4$:Er^{3+},Yb^{3+} hexagonal crystals from microtubes to microprisms and eventually nanobarrels as reported in other relevant systems. For example, Zhang *et al.*[11] found that the upconversion emission intensity of Er^{3+},Yb^{3+}-doped-hexagonal nanocrystals (nanorods, nanotubes or nanodiscs) prepared in the presence of oleic acid (as capping agent) was as much as 50% lower than the corresponding one of bulk crystals of the same composition. This size-dependent reduction in upconversion intensity of oleic acid-capped nanocrystals has been shown to arise from a surface quenching effect.[9] However, it is interesting to note that Sun *et al.*[12a] found the upconversion luminescence of 1–2 μm hexagonal crystals prepared with citrate to be weaker than that of nanosized crystals prepared with EDTA as complexing agent. This implies that the observed decrease in total emission is not only due to crystal size reduction but could arise as well from the surface adsorbed carboxylate (citrate or oleic in other studies[11,22]) groups. In this context it has been shown earlier that high-energy vibrational modes such as OH in the citrate molecule can lead to quenching of the excited lanthanide states by multiphonon relaxation processes.[23] Further indirect evidence of this effect is presented in the subsequent annealing section. Although citrate had a negative impact on total emission, its presence was found to increase the green-to-red emission ratio above one (see unannealed citrate samples C2–C5 with citrate-free samples #2 and #3). It appears that when the {0001} facets are inhibited, the green emission is enhanced. This may provide a path to tune the green-to-red ratio for specific applications, such as dye-sensitized solar cells that absorb green light better than red light.[5a]

3.2 Ultra-efficient up-converting $NaYF_4$:Er^{3+},Yb^{3+} crystals *via* annealing

Annealing is investigated and shown here for the first time to play a critical role in engineering ultra-efficient NIR-to-visible upconversion $NaYF_4$:Er^{3+},Yb^{3+} crystals.

3.2.1 Effect of annealing on crystal structure. The various hydrothermally synthesized $NaYF_4$:Er^{3+},Yb^{3+} crystals were annealed for 2 h at 350 and 700 °C and subsequently characterized by Raman spectroscopy to help explain the effect of annealing on upconversion luminescence. All Raman spectra are provided in Fig. S3 of the ESI,† while the upconversion data as a function of annealing temperature is summarized in Table 2. As mentioned in the previous section, hexagonal structured crystals displayed six strong characteristic Raman peaks while the cubic structured crystals showed two very broad peaks in the range of 800 and 1400 cm^{-1} independent of the presence of citrate. According to their Raman spectra, the cubic (α) structure crystals (#1 and C1; refer to Fig. S2 in ESI†) showed no phase change after annealing. This observation was corroborated by XRD (in the case of sample #1, see Fig. S1, ESI†). The hexagonal crystals responded differently to annealing depending on the use of citrate during their hydrothermal synthesis. The citrate-free hexagonal crystals (samples #2 and #3) maintained hexagonal structure after annealing at 350 °C but converted to cubic structure (α-$NaYF_4$:Er^{3+},Yb^{3+}) after annealing at 700 °C (see spectra in Fig. 4 and S3, ESI†). Yi *et al.*[24] have similarly reported that hexagonal phase converts fully to cubic phase when heated to 700 °C. Thomas *et al.* also reported that above 700 °C

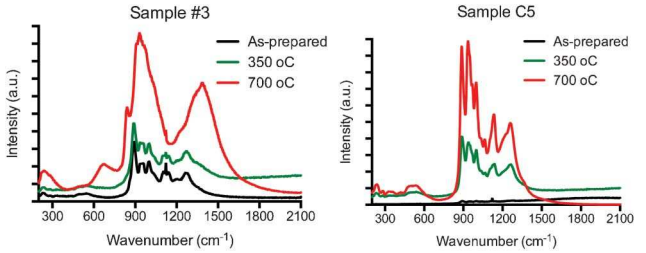

Fig. 4 Raman spectra of citrate-free (sample #3) and citrate-modified (sample C5) $NaYF_4$:Er^{3+},Yb^{3+} crystals before (as-prepared, black) and after annealing at 350 °C (green) and 700 °C (red).

the hexagonal phases of iso-structural $NaPrF_4$ and $NaLuF_4$ compounds convert to disordered fluorite-like cubic phases of variable composition.[25] However, the citrate-modified β-phase crystals (samples C2–C5) did not convert to α-phase $NaYF_4$:Er^{3+},Yb^{3+} even after annealing at 700 °C, indicating the citrate molecules suppress the β-to-α phase transition. The suppression has been reported by Yi *et al.*[24] where EDTA was used as chelating reagent. Another interesting observation that can be made is that the annealed crystals in Fig. 4 have sharper and more intense Raman peaks than those of as-prepared ones. This is attributed to crystal refinement and improved crystallinity *via* defect removal as result of facilitated atom diffusion. Finally annealing induced crystal growth and partial sintering resulting in morphology alteration from individual prismatic crystals (Fig. 1 (C3)) to irregular agglomerates (see Fig. S4 of the ESI†). Hence the annealed crystals were ground prior to measurement of their upconversion response (section 3.2.2).

3.2.2 Effect of annealing on upconversion response. The beneficial effect of annealing on the upconversion response of $NaYF_4$:Er^{3+},Yb^{3+} crystals is exemplified with the typical luminescence spectra (sample C2) shown in Fig. 5. It is clear that the intensity of UC luminescence (both green and red emissions) increased when samples were annealed at 350 °C or 700 °C. Comparison of the UC spectra of Fig. 5 with the Raman spectra of Fig. 4 reveals a striking correlation with annealing

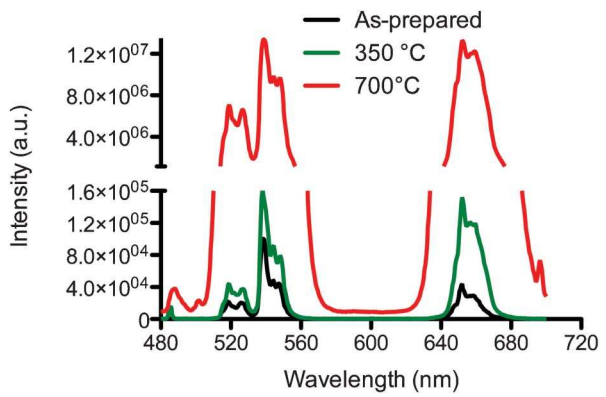

Fig. 5 Upconversion emission spectra of citrate-modified β-$NaYF_4$:Er^{3+},Yb^{3+} crystals (sample C2) following hydrothermal synthesis (as-prepared), and after annealing at 350 °C and 700 °C.

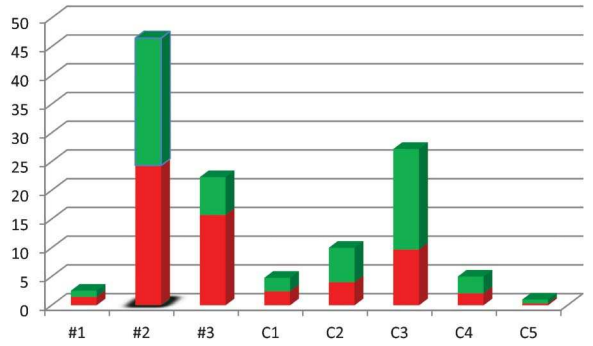

Fig. 6 Total upconversion and green/red intensity of as-prepared $NaYF_4$:Er^{3+},Yb^{3+} crystals.

simultaneously increasing both Raman peak intensities and luminescence.

A complete summary of upconversion intensities and the green-to-red ratios of annealed $NaYF_4$:Er^{3+},Yb^{3+} crystals is presented in Table 2. Total upconversion intensity of as-prepared samples, and samples annealed at 350 °C and 700 °C are compared in Fig. 6 and 7. As can be seen in Table 2 and Fig. 7, the upconversion intensity of the citrate-free crystals (samples #1–#3) increased upon annealing at 350 °C. The upconversion intensity of sample #2 annealed at 350 °C is 25-times higher compared to that of the as-prepared sample. This increase corresponds to 21.4 and 29.3 times enhancement of the sample's green and red emission, respectively. Interestingly, the upconversion intensity of the small-sized cubic crystals of sample #1 increased over 160 times after annealing at 350 °C. Similarly, the upconversion intensities of citrate-modified hexagonal crystals (samples C2, C4, and C5 with the exception of sample C3) also increased. However, the observed increase in emission intensity with annealing at 350 °C was at the partial detriment of the green-to-red ratios of all samples, decreasing the green emission relative to red.

Annealing at 700 °C resulted in further increase in upconversion intensities. The total emission intensities for

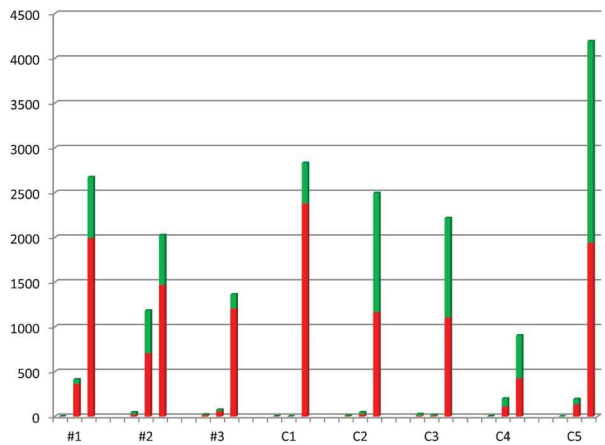

Fig. 7 Total and green/red upconversion intensity of as-prepared (left), 350 °C-annealed (middle), and 700 °C-annealed (right) $NaYF_4$:Er^{3+},Yb^{3+} crystals.

these samples were 20–90 times higher than that of the as-prepared sample #2 used as reference. The increase in luminescence intensity paralleled the increase of Raman peak intensity as evident from the spectra in Fig. 4. Both the intensity of the Raman peaks as well as the UC luminescence increase when samples are annealed at 350 °C or 700 °C. As shown in Table 2, the annealing-induced UC intensity enhancement is greater for the small-sized crystals. The largest emission enhancement from annealing was in the nano/sub-micron scale hexagonal crystal sample C5 (~150–200 nm barrel-like crystals), which was over 4000 times stronger than its as-prepared counterpart (a total emission intensity of ~90 a.u.), much higher than that of microsized crystals. This sample also had the highest green-to-red ratio of all the samples annealed at 700 °C. This is a remarkable discovery since small (nano-submicron) sized crystals suffer from lower emission intensity due to surface quenching.[9] It is postulated that annealing at 700 °C improves the upconversion efficiency of the crystals *via* elimination of surface hydroxyl (and citrate groups) endowed in the crystals from the hydrothermal synthesis environment, as these are known to increase the multi-phonon relaxation rates between the metastable states thus reducing the overall visible emission intensity.[11] Annealing under the right conditions (700 °C and 2 h) is also believed to create an internally defect-free structure. Defects are known to cause weak luminescence due to dissipation of the upconverted state in the dopant ion.[9]

Another notable result is the strong upconversion intensity observed in the cubic structured samples annealed at 700 °C, which were of the same order of magnitude or higher than that of the hexagonal structured samples. Cubic $NaYF_4$:Er^{3+},Yb^{3+} crystals are often observed to be poor upconverters compared to hexagonal counterparts and this is the first time such strong emission is observed in cubic crystals. The key difference between the cubic and hexagonal crystal varieties (after annealing at 700 °C) is their relative green and red emissions with hexagonal (especially sample C5) being a green emitter and cubic (C1) a red emitter.

The role of citrate deserves some final discussion. *Via* preferential adsorption, when in large excess, citrate helps control crystal growth hence produce nano/submicron scale crystals. As-prepared by hydrothermal synthesis crystals suffer from low luminescence due not only to the small size but also due to the organic citrate and OH surface groups. Upon annealing at 700 °C (350 °C apparently is not high enough) the citrate surface groups are eliminated resulting in greatly improved UC emission.

4 Conclusions

Nano-/micro-scale $NaYF_4$:Er^{3+},Yb^{3+} crystals with ultra-efficient upconversion of NIR-to-VIS were obtained *via* annealing following citrate-assisted hydrothermal synthesis at 200 °C. Both hexagonal (β) and cubic (α) crystals were produced. The crystallization process involved α-to-β phase transition *via* the dissolution–recrystallization mechanism. Raman spectroscopy was employed for the first time to distinguish between the two phases taking advantage of the different peaks exhibited in the range of 800 and 1400 cm^{-1}. Citrate acted as complexing agent, regulating the nucleation of α (cubic) crystallites as well as crystal modifier, controlling α and β crystal growth. Citrate in combination with the right Fluoride-F/RE (where RE = Y + Er + Yb) molar ratio was shown to stabilize both the α (F/RE = 4) and β (F/RE = 9) crystals depending on conditions. As a result nanosized (~20 nm) α crystallites were produced. Similarly, citrate modified the morphology of the β phase crystals from elongated microtubes (1D growth) to hexagonal prisms (2D growth). With increasing citrate concentration the hexagonal prism crystals became progressively smaller and more isometric. Use of citrate-assisted crystal modification led to significant deterioration of the upconversion luminescence of the β $NaYF_4$:Er^{3+},Yb^{3+} crystals that was linked to surface quenching arising from adsorbed citrate moieties. Despite this decrease, the citrate additive was found to increase the green-to-red emission ratio above 1.

Annealing the crystals at 700 °C allowed upconversion efficiencies to be dramatically enhanced (over three orders of magnitude), and the green-to-red ratio to be tuned. The most remarkable enhancement was observed in the citrate-modified sub-micron-sized hexagonal crystal sample (~150–200 nm sized spheroids), which after annealing at 700 °C yielded upconversion intensity over 4000 times stronger than that of its as-prepared counterpart. It is proposed that annealing at 700 °C improves the upconversion efficiency of the crystals *via* creation of an internally defect-free structure and *via* elimination of surface groups left from the citrate-assisted hydrothermal treatment.

Acknowledgements

The work described here was funded through the strategic project grant program of NSERC (the Natural Sciences and Engineering Research Council of Canada).

Notes and references

1 (*a*) F. Wang, R. Deng, J. Wang, Q. Wang, Y. Han, H. Zhu, X. Chen and X. Liu, *Nat. Mater.*, 2011, **10**(12), 968; (*b*) M. Haase and H. Schäfer, *Angew. Chem., Int. Ed.*, 2011, **50**, 5808; (*c*) Y. Park, J. H. Kim, K. T. Lee, K. Jeon, H. B. Na, J. H. Yu, H. M. Kim, N. Lee, S. H. Choi, S. Baik, H. Kim, S. P. Park, B.-J. Park, Y. W. Kim, S. H. Lee, S.-Y. Yoon, I. C. Song, W. K. Moon, Y. D. Suh and T. Hyeon, *Adv. Mater.*, 2009, **21**, 4467.

2 F. Wang, Y. Han, C. S. Lim, Y. H. Lu, J. Wang, J. Xu, H. Y. Chen, C. Zhang, M. H. Hong and X. G. Liu, *Nature*, 2010, **463**, 1061.

3 C. Zhang, H. P. Zhou, L. Y. Liao, W. Feng, W. Sun, Z. X. Li, C. H. Xu, C. J. Fang, L. D. Sun, Y. W. Zhang and C.-H. Yan, *Adv. Mater.*, 2010, **22**, 633.

4 (*a*) C. Li and J. Lin, *Mater. Chem. Phys.*, 2010, **20**, 6831; (*b*) M. He, P. Huang, C. Zhang, H. Hu, C. Bao, G. Gao, R. He and D. Cui, *Adv. Funct. Mater.*, 2011, **21**, 4470.

5 (*a*) G. Shan, H. Assaaoudi and G. P. Demopoulos, *ACS Appl. Mater. Interfaces*, 2011, **3**, 3239; (*b*) J. Wu, J. Wang, J. Lin, Z. Lan, Q. Tang, M. Huang, Y. Huang, L. Fan, Q. Li and Z. Tang, *Adv. Energy Mater.*, 2012, **2**, 78–81.
6 (*a*) F. Auzel, *Chem. Rev.*, 2004, **104**, 139; (*b*) M. Haase and H. Schäfer, *Angew. Chem., Int. Ed.*, 2011, **50**, 5808.
7 J. F. Suyver, J. Grimm, M. K. van Veen, D. Biner, K. W. Krãmer and H. U. Gudel, *J. Lumin.*, 2006, **117**, 1.
8 K. W. Krämer, D. Bine, G. Frei, H. U. Güdel, M. P. Hehlen and S. R. Lüthi, *Chem. Mater.*, 2004, **16**, 1244.
9 F. Wang, J. Wang and X. Liu, *Angew. Chem., Int. Ed.*, 2010, **49**, 7456.
10 (*a*) Z. Li, Y. Zhang and S. Jiang, *Adv. Mater.*, 2008, **20**, 4765; (*b*) X. Ye, J. E. Collins, Y. Kang, J. Chen, D. T. N. Chen, A. G. Yodh and C. B. Murray, *Proc. Natl. Acad. Sci. U. S. A.*, 2010, **28**, 22430.
11 F. Zhang, J. Li, J. Shan, L. Xu and D. Zhao, *Chem.–Eur. J.*, 2009, **15**, 11010.
12 (*a*) Y. Sun, Y. Chen, L. Tian, Y. Yu, X. Kong, J. Zhao and H. Zhang, *Nanotechnology*, 2007, **18**(27), 275609; (*b*) Z. H. Ni, H. M. Wang, Y. Ma, J. Kasim, Y. H. Wu and Z. X. Shen, *ACS Nano*, 2008, **2**(5), 1033; (*c*) C. Li, J. Yang, P. Yang, X. Zhang, H. Lian and J. Lin, *Cryst. Growth Des.*, 2008, **8**(3), 923.
13 F. Hund, *Z. Anorg. Allg. Chem.*, 1950, **263**, 102.
14 A. Grzechnik, P. Bouvier, M. Mezouar, M. D. Mathews, A. K. Tyagi and J. Köhler, *J. Solid State Chem.*, 2002, **165**, 159.
15 G. P. Demopoulos, *Hydrometallurgy*, 2009, **96**, 199.
16 A. Huignard, V. Buissette, G. Laurent, T. Gacoin and J.-P. Boilot, *Chem. Mater.*, 2002, **14**, 2264.
17 Y. Wang, R. Cai and Z. Liu, *CrystEngComm*, 2011, **13**, 1772.
18 J. A. Dirksen and T. A. Ring, *Chem. Eng. Sci.*, 1991, **46**, 2389.
19 H. Mai, Y. Zhang, R. Si, Z. Yan, L. Sun, L. You and C. Yan, *J. Am. Chem. Soc.*, 2006, **128**, 6426.
20 A. Tian, K. Voigt, J. Liu, B. Mckenzie, M. J. Mcdermott, M. R. Rodriguez, H. Konishi and H. F. Xu, *Nat. Mater.*, 2003, **2**, 821.
21 C. Renero-Lecuna, R. Martin-Rodriguez, R. Valiente, J. Gonzalez, F. Rodriguez, K. W. Krämer and H. U. Güdel, *Chem. Mater.*, 2011, **23**, 3442.
22 T. Cao, T. Yang, Y. Gao, Y. Yang, H. Hu and F. Li, *Inorg. Chem. Commun.*, 2010, **13**, 392.
23 K. Riwotzki, H. Meyssamy, H. Schnablegger, A. Kornowski and M. Haase, *Angew. Chem., Int. Ed.*, 2001, **40**, 573.
24 G. S. Yi, H. C. Lu, S. Y. Zhao, G. Yue, W. J. Yang, D. P. Chen and L. H. Guo, *Nano Lett.*, 2004, **4**, 2191.
25 R. E. Thomas, H. Insley and G. M. Hebert, *Inorg. Chem.*, 1966, **5**, 1222.

